ISSN 1392-1207. MECHANIKA. Vol. 30, No. 6, 2024: 507–513

Optimization of Restrictor Parameters and Static Characteristics Study on Orifice Type Hydrostatic Thrust Bearing

Yuanlong CHEN*, Xinyu WEN, Yuqing WANG***, Muyao WU****, Jiarui ZHOU*****, Shaoqi WANYAN******

**School of Mechanical Engineering, Hefei University of Technology, 230009 Hefei, China,*
E-mail: chenyuanlong@hfut.edu.cn (Corresponding author)
***School of Mechanical Engineering, Hefei University of Technology, 230009 Hefei, China,*
E-mail: 18865721932@163.com
****School of Mechanical Engineering, Hefei University of Technology, 230009 Hefei, China,*
E-mail: yuqingw@hfut.edu.cn
*****School of Automotive Engineering, Hefei University of Technology, 230009 Hefei, China,*
E-mail: wumuyao@hfut.edu.cn
******School of Mechanical Engineering, Hefei University of Technology, 230009 Hefei, China,*
E-mail: 707540051@qq.com
*******School of Mechanical Engineering, Hefei University of Technology, 230009 Hefei, China,*
E-mail: 1360180610@qq.com

https://doi.org/10.5755/j02.mech.37282

1. Introduction

The ultra-precision machine tool is an essential tool for achieving ultra-precision machining, which holds significant importance in the advancement of chip, energy, aerospace, and other related fields [1-4]. The spindle, being a critical component of ultra-precision machine tools, faces challenges in meeting the requirements of high velocity and stability using traditional rolling bearings. Gas bearings have gained attention from scholars worldwide due to their advantages such as high rotational velocity, precision, and durability [5-7]. The static load carrying performance of hydrostatic bearings was slightly insufficient when compared to liquid lubricated bearings.

In order to enhance the load-carrying-capacity of hydrostatic gas bearings, numerous scholars have conducted thorough research. Sahto et al. [8] conducted modeling and simulation studies on different types of aerostatic thrust bearings, including porous, orifice, and multiple type bearings. Yu et al. [9] examined the impact of various factors, including the thickness of the porous material, working surface error, and rotational velocity, on the static characteristics of circular thrust bearings. Cui et al. [10] analyzed the effects of various factors such as excitation amplitude, excitation frequency, axial eccentricity ratio, and non-flatness on the dynamic performance of these bearings using a dynamic mesh technique. Khan et al. [11] analyzed the pressure distribution, radial load, and thrust load patterns in relation to the percentage of porous material, permeability, and eccentricity. Nishio et al. [12] conducted experimental and numerical studies on aerostatic annular thrust bearings equipped with diameters of throttle orifice below 0.05 mm.

In the context of orifice restrictor bearings, the PEG serves to decrease the pressure decay rate away from the orifice restrictor, thereby balancing the pressure distribution and ultimately improving the overall carrying-capacity of the gas film. Present research primarily concentrated on examining the impact of individual factor modifications on the bearing capacity of gas bearings, with limited investigation into the combined effects of multiple structural parameters of the restrictor. ANSYS Fluent was utilized to comprehensively evaluate the influence of the restrictor and the structural parameters of PEG on the static load-carrying-capacity of the bearing in this research. The range analysis and ANOVA were done to analyze the experimental data, with an aim to identify the optimal combinations of structural parameters that yield the best static load carrying performance. The findings from this research endeavor aim to provide valuable insights for the advancement of annular hydrostatic gas thrust bearings with improved bearing capacity.

2. Bearing model

The orifice restrictor bearing model selected in this research is shown in Fig. 1. The outer diameter of the bearing D = 70 mm, the position of the orifice restrictor D_1 = 52 mm and the inner diameter of the bearing D_2 = 35 mm. Gas is introduced into the bearing through the gas supply orifice, and upon traversing the restrictor, a consistent gas film is established between the bearing and the thrust plate, effectively facilitating the support of the thrust plate.

The ANSYS Fluent 2021 software was utilized to carry out the fluid simulation. The fluid domain model for simulation was created by extracting the gas film between the bearing and thrust plate. This is illustrated in Fig. 2, a.

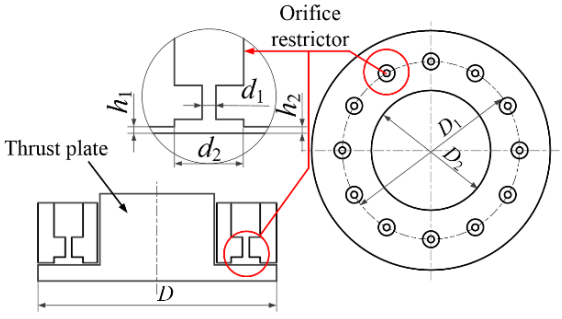

Fig. 1 Bearing model

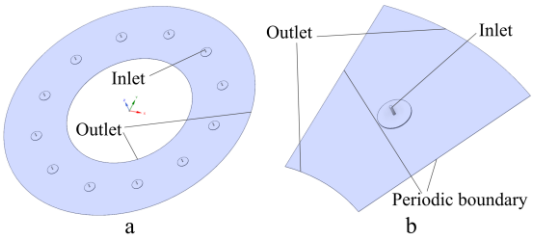

Fig. 2 Fluid simulation models: a – fluid domain model, b – boundary conditions

The bearing comprised 12 gas supply orifice that were symmetrically distributed [13]. Each gas supply orifice corresponds to a cylindrical PEG located below. To reduce the simulation time, a fraction of the flow field, specifically 1/12, was selected for simulation as shown in Fig. 2, b. The two sides of the flow field were designated as periodic boundaries to ensure accurate simulation results. The boundary conditions for the flow field are presented in Fig. 2, b. The unlabeled section was defined as the wall.

3. Simulation Experimental Methodology and Design

3.1. Simulation experimental methodology

This study utilized an ideal gas as a simulated medium, with simulation computational conditions and fluid parameters detailed in Table 1. The quality of the grid significantly impacts the computational results. To enhance grid quality and ensure accuracy in calculations, a hexahedral structural grid was employed. The gas film grid and magnified image are illustrated in Fig. 3, a, where the gas film is partitioned into three sections for grid generation to improve grid quality. The orthogonal quality of the generated grid is depicted in Fig. 3, b.

The accuracy of calculation results was influenced by the mesh quality. Increasing the density of the mesh led to more precise calculation results; however, this also

Table 1

Computational conditions and fluid parameters

Parameters	Value
Supply pressure	0.6 MPa
Outlet pressure	0.1 MPa
Atmospheric pressure	101.325 kPa
Temperature	300 K
Method of solution	Simple C
Solution standardization	Standard initialization
Fluid	Ideal gas
Viscosity flow	Laminar
Density	1.225 kg/m^3
Specific heat	1006.34 J/(kg·K)
Thermal conductivity	0.0242 W/(m·K)
Dynamic viscosity	1.7894e^{-5} kg/(m·s)

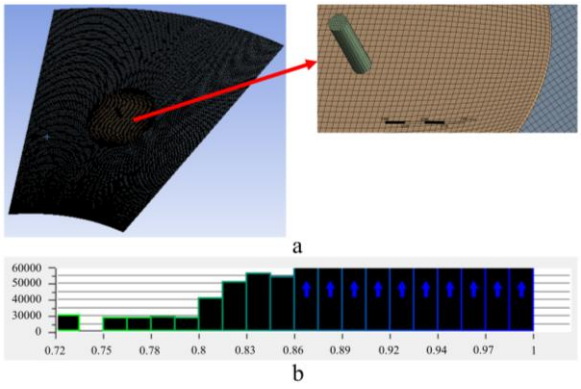

Fig. 3 Mesh model of aerostatic thrust bearing: a – gas film grid, b – orthogonal quality of the generated grid

resulted in a considerable increase in workload and calculation time. Therefore, it was not advisable to solely rely on increasing mesh density as a means to enhance calculation accuracy. It was more prudent to select an appropriate number of meshes that correspond to the actual model. This strategy not only saved computation time but also ensured accurate results. In this study, mesh independence was verified based on the actual bearing model, as shown in Fig. 4. As the number of meshes increased, the LCC of the gas bearing gradually decreased. However, once the number of meshes surpassed 1.2 million, the LCC stabilized, with the variation being controlled within 1%. Consequently, it can be inferred that the impact of the number of meshes on calculation accuracy was minimal at this juncture. It was determined that approximately 1.2 million meshes should be utilized in the simulation process.

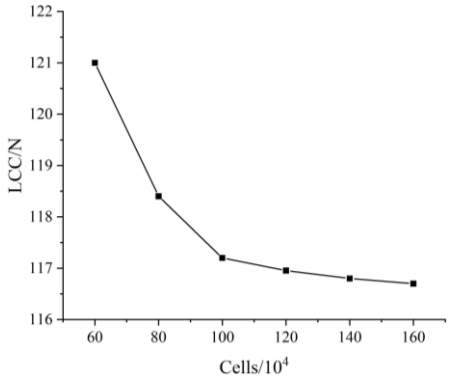

Fig. 4 Mesh-independent verification

3.2. Simulation experimental design

Diameter of orifices d_1, thickness of gas film h_1, PEG diameter d_2, and PEG depth h_2 were selected as experimental factors. Table 2 displays the specific parameters and corresponding levels. The Taguchi method was used to arrange the L16 orthogonal test to explore the influence of

Table 2

Input parameters and their levels for restrictors

Parameters	Level 1	Level 2	Level 3	Level 4
Diameter of orifices d_1	0.10 mm	0.15 mm	0.20 mm	0.25 mm
Thickness of gas film h_1	0.010 mm	0.015 mm	0.020 mm	0.025 mm
PEG diameter d_2	2 mm	3 mm	4 mm	5 mm
PEG depth h_2	0.03 mm	0.05 mm	0.07 mm	0.09 mm

Table 3

L-16 orthogonal array

Run	Processing parameters				Response indicators	
	d_1 mm	h_1 mm	d_2 mm	h_2 mm	LCC N	MFR g/s
1	0.10	0.010	2	0.03	166.955	0.0697
2	0.10	0.015	3	0.05	78.167	0.0866
3	0.10	0.020	4	0.07	58.407	0.0946
4	0.10	0.025	5	0.09	21.089	0.1006
5	0.15	0.010	3	0.07	395.840	0.1456
6	0.15	0.015	2	0.09	192.726	0.1633
7	0.15	0.020	5	0.03	87.186	0.1904
8	0.15	0.025	4	0.05	55.941	0.2010
9	0.20	0.010	4	0.09	516.247	0.2108
10	0.20	0.015	5	0.07	374.811	0.2914
11	0.20	0.020	2	0.05	152.498	0.2933
12	0.20	0.025	3	0.03	81.275	0.3390
13	0.25	0.010	5	0.05	656.922	0.2676
14	0.25	0.015	4	0.03	321.838	0.3346
15	0.25	0.020	3	0.09	250.826	0.4645
16	0.25	0.025	2	0.07	188.252	0.5046

various parameter combinations on LCC and MFR. The implementation of orthogonal Taguchi design proved to be an effective strategy for enhancing experimental efficiency and upholding the precision of the experiment, all the while minimizing the experimental size [14-16]. The impact of different combinations of parameters on the LCC and MFR was investigated by analyzing the simulation results using the Fluent post. It was important to note that, while conducting the simulations, all other parameters remained constant. The simulation test program and the corresponding results are provided in Table 3. The LCC and MFR were output from the fluent post-processor.

4. Result and Discussion

The impact of restrictor structural parameters on the response index was conducted through the analysis of test results using ANOVA methods. LCC, in general, pertains to the static load-carrying-capacity of the bearing, while MFR signifies the gas consumption experienced during the operational procedure. Consequently, a gas bearing restrictor that exhibits a high LCC and a low MFR assumes significance as it serves as a crucial factor in augmenting the overall performance of the bearings.

4.1. Effect of different parameters on LCC

Range analysis and ANOVA tables of LCC mode are presented in Tables 4 and 5, respectively. Table 4 revealed that the order of precedence for the four factors influencing LCC was as follows: thickness of gas film, diameter of orifices, PEG diameter, and PEG depth. According to the findings presented in Table 5, it was evident that the LCC model held great significance. Additionally, the impacts of variables such as diameter of orifices, thickness of gas film, and PEG diameter on LCC were also found to be significant. However, the effect of PEG depth on LCC was not deemed significant. Interestingly, the LCC reached its peak value when the diameter of orifices measured 0.25 mm, the thickness of gas film was 0.01 mm, the PEG diameter was 5 mm, and the PEG depth was 0.07 mm. Fig. 5 depicts the impact of various structural parameters of the restrictor on the LCC. It revealed that as the diameter of orifices and the PEG diameter increased, the LCC exhibited consistent linear growth. Moreover, the rate of LCC increased due to changes in diameter of orifices was found to be higher. However, when the thickness of gas film increased, the LCC demonstrated a linear decline. Additionally, the LCC displayed an initial increase followed by a decrease as the PEG depth increased, reaching its maximum value at a depth of 0.07 mm.

The impact of the interplay between the thickness of gas film and the remaining three factors on the LCC is demonstrated in Fig. 6. Notably, Fig. 6 illustrated that the thickness of the gas film exerted a substantial influence on the LCC, with a distinct downward trajectory observed as the gas film thickness increased. This can be attributed to

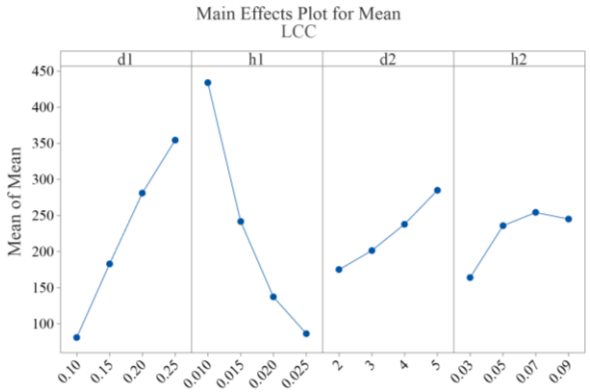

Fig. 5 Effect of different factors on LCC

Table 4

Range for LCC

		d_1	h_1	d_2	h_2
LCC	K_1	324.618	1735.964	700.431	657.254
	K_2	731.693	967.542	806.108	943.528
	K_3	1124.831	548.917	952.433	1017.310
	K_4	1417.838	346.557	1140.008	980.888
	R	1093.220	1389.407	439.577	360.056

Table 5

ANOVA for LCC

Source	Adj SS	*df*	Adj MS	*F* value	*P* value	Significance
Model	5.003E+005	12	41691.11	43.08	0.0051	*
A-d_1	1.695E+005	3	56508.05	58.39	0.0037	*
B-h_1	2.832E+005	3	94412.99	97.55	0.0017	*
C-d_2	27249.07	3	9083.02	9.39	0.0492	*
D-h_2	20281.14	3	6760.38	6.99	0.0723	
Residual error	2903.41	3	967.80			
Total	5.032E+005	15				

'*' - $0.0001 \leq P \leq 0.05$, significant. $P \geq 0.05$, not significant

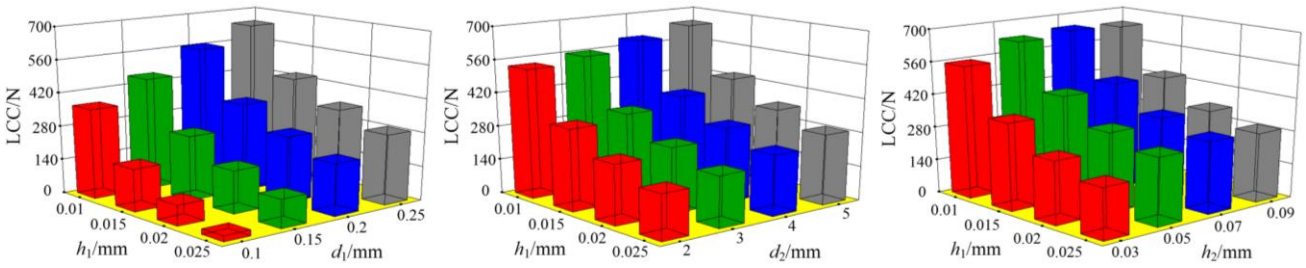

a b c

Fig. 6 Interaction of different factors on LCC. a – LCC versus h_1 and d_1 under d_2=5 mm and h_2=0.05 mm, b – LCC versus h_1 and d_2 under d_1 = 0.25 mm and h_2 = 0.05 mm, c – LCC versus h_1 and h_2 under d_1 = 0.25 mm and d_2 = 5 mm

the expanding gap between the bearings and the consequent enlargement of the compressed gas flow space, resulting in an elevated pressure drop. Consequently, there was a discernible decline in the LCC. Fig. 6, a exhibited a positive correlation between the bearing capacity and the diameter of orifices, indicating an increasing trend. Conversely, Fig. 6, b suggested that the widening of the PEG diameter did not significantly affect the increase in the LCC within the selected parameter range. Furthermore, Fig. 6, c illustrates that the LCC initially rose and then declined as the PEG depth increased, with an inflection point occurring at h_2 = 0.07 mm. The behavior may be attributed to the formation of eddy currents within the PEG, resulting in a reduction of the LCC when the depth was excessively large.

4.2. Effect of different parameters on MFR

Tables 6 and 7 present the range analysis and ANOVA tables, respectively, for the MFR model. According to the findings in Table 6, the four factors that impacted the MFR were ranked in the following order of priority: diameter of orifices, thickness of gas film, PEG diameter, and PEG depth. Table 7 revealed that the MFR model was statistically significant, with the diameter of orifices having a significant effect on MFR. However, the effects of thickness of gas film, PEG diameter, and PEG depth on MFR were not statistically significant. The MFR was minimized when the diameter of orifices was 0.1 mm, the thickness of gas film was 0.01 mm, the PEG diameter was 4 mm, and the PEG depth was 0.05 mm. The results presented in Fig. 7 demonstrated the impact of various structural parameters of the restrictor on the MFR. As the diameter of orifices and thickness of gas film increased, the MFR exhibited a consistent linear growth. However, it was worth noting that changes in the diameter of orifices resulted in a more pronounced rate of MFR increase. In contrast, PEG diameter and PEG depth led to a relatively negligible effect on the MFR, as evidenced by the floating trend within a specific range. These findings suggested that the influence of the diameter and depth of PEG on the MFR was of limited significance.

The influence of the diameter of orifices, in conjunction with the remaining three variables, on the mass flow rate MFR was depicted in Fig. 8. It was evident from Fig. 8 that the diameter of orifices had a significant impact on the MFR. Specifically, as the diameter of orifices increased, there was a distinct upward trajectory observed in the MFR. This can be attributed to the fact that the enlargement of the diameter of orifices augmented the cross-sectional area through which the gas passed per unit time, consequently leading to an amplified MFR. Fig. 8, a demonstrated that the MFR exhibited an increase as the thickness of gas film increased. This can be attributed to the fact that

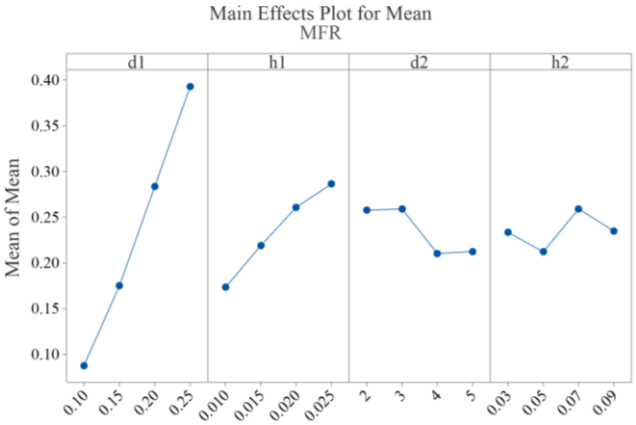

Fig. 7 Effect of different factors on MFR

Table 6

Range for MFR

		d_1	h_1	d_2	h_2
MFR	K_1	0.3514	0.6937	1.0309	0.9337
	K_2	0.7003	0.8758	1.0356	0.8484
	K_3	1.1345	1.0428	0.8410	1.0361
	K_4	1.5713	1.1451	0.8500	0.9392
	R	1.2199	0.4514	0.1946	0.1877

Table 7

ANOVA for MFR

Source	Adj SS	*df*	Adj MS	*F* value	*P* value	Significance
Model	0.25	12	0.021	12.44	0.0306	*
A-d_1	0.21	3	0.070	41.36	0.0061	*
B-h_1	0.029	3	9.786E-003	5.78	0.0918	
C-d_2	8.832E-003	3	2.944E-003	1.74	0.3303	
D-h_2	4.415E-003	3	1.472E-003	0.87	0.5445	
Residual error	5.078E-003	3	1.693E-003			
Total	0.26	15				

'*' - $0.0001 \leq P \leq 0.05$, significant. $P \geq 0.05$, not significant

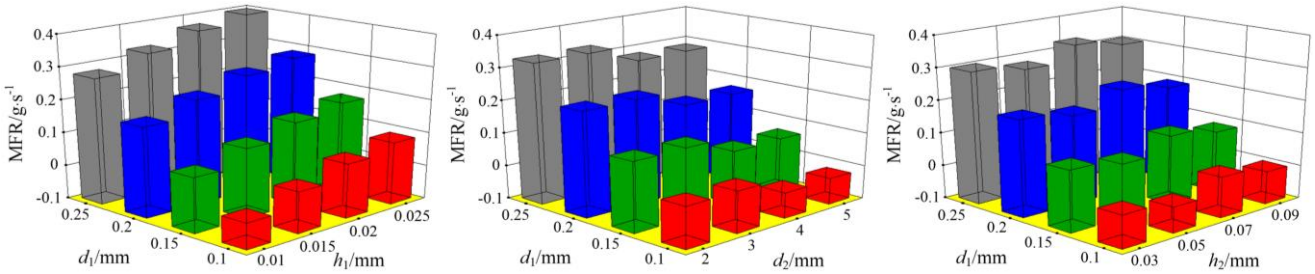

a b c

Fig. 8 Interaction of different factors on MRF: a – MRF versus d_1 and h_1 under d_2 = 4 mm and h_2 = 0.05 mm, b – MRF versus d_1 and d_2 under h_1 = 0.01 mm and h_2 = 0.05 mm, c – MRF versus d_1, h_2 under h_1 = 0.01 mm and d_2 = 4 mm

an increase in the gas film thickness led to a wider gap between the bearings, resulting in a larger space for high pressure gas within the bearings. Consequently, the MFR displayed an upward trend. In Fig. 8, b, c, it can be observed that the MFR experienced minor fluctuations within a certain range as the diameter and depth of PEG increased. Thiscan be attributed to the fact that the incremental changes in the width and depth of the homogenizing groove were relatively small, thus having a negligible impact on the MFR.

4.3. Optimization of parameters

The optimal configuration of restrictor structural parameters to achieve the best LCC, as identified in the preceding section, consisted of diameter of orifices d_1 = 0.25 mm, thickness of gas film h_1 = 0.01 mm, PEG diameter d_2 = 5 mm, and PEG depth h_2 = 0.07 mm. Additionally, the most favorable combination of restrictor structure parameters for achieving the optimum MFR entailed diameter of orifices d_1 = 0.10 mm, thickness of gas film h_1 = 0.01 mm, PEG diameter d_2 = 4 mm, and PEG depth h_2 = 0.05 mm.

The enhancement of bearing static load capacity is primarily manifested by the increase in LCC. However, the increase in LCC inevitably leads to an increase in gas consumption, resulting in an elevation of MFR. Since LCC serves as a vital indicator for evaluating the bearing load capacity, selecting the optimal LCC as the parameter optimization target is crucial. Nonetheless, it is imperative to ensure that MFR exhibits a minimal growth rate to guarantee lower gas consumption. This study models the restricted parameter combination under the optimal conditions of LCC and conducts simulated verification tests. The results of the simulation tests are presented in Table 8. By comparing the optimal value of the index obtained in the orthogonal test before parameter optimization, it was observed that the LCC increased by 8% after the parameter optimization, while the MFR only experienced a 3% rise. This suggested that there was no significant increase in gas consumption. The cloud diagram of the gas film pressure distribution shown in Fig. 9 illustrates the changes before and after parameter optimization. It is evident that the pressure decreases in a gradient manner from the air supply orifice towards both sides. The peak pressure of gas film after optimization shows a certain level of improvement compared to the pressure before optimization. Fig. 10, on the other hand, demonstrates the pressure distribution curve along a straight line at the bottom of the gas film. It can be inferred that the parameter optimization led to an increase in pressure values at various points within the cross-section. This increase in pressure was also

Table 7

ANOVA for MFR

Indicator	LCC	MFR
before optimization	656.922 N	0.0655 g/s
after optimization	709.476 N	0.0674 g/s
percentage	8%	3%

responsible for the observed rise in LCC. By employing the best LCC as the guiding principle for optimization, the ultimate choice for the thickness of gas film of the bearing was determined to be h_1=0.01 mm. In addition, the structural parameters of the restrictor were determined as follows: diameter of orifices d_1=0.25 mm, PEG diameter d_2=5 mm, and PEG depth h_2=0.07 mm. These specific parameters were found to enable the bearing to achieve its optimal static load-carrying-capacity.

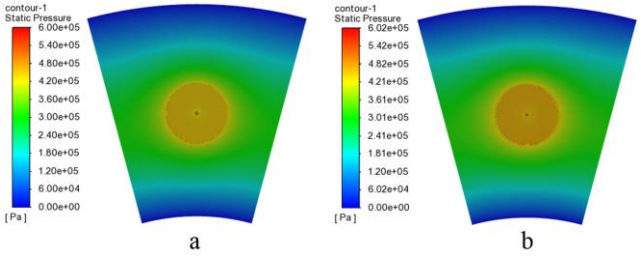

a b

Fig. 9 Gas film pressure distribution. a – before optimization; d_1 = 0.25 mm, h_1 = 0.01 mm, d_2 = 5 mm, h_2 = 0.05 mm, b – after optimization; d_1 = 0.25 mm, h_1 = 0.01 mm, d_2 = 5 mm, h_2 = 0.07 mm

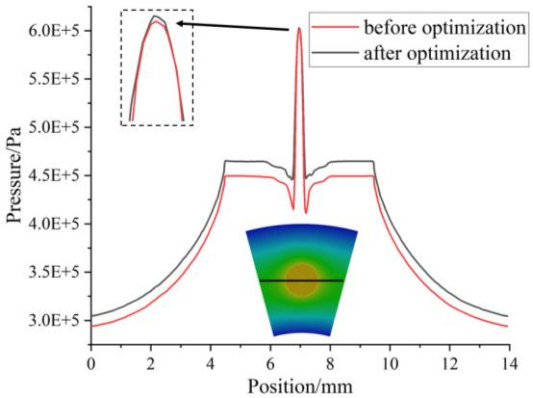

Fig. 10 Pressure distribution curve: before optimization: d_1 = 0.25 mm, h_1 = 0.01 mm, d_2 = 5 mm, h_2 = 0.05 mm, after optimization: d_1=0.25 mm, h_1 = 0.01 mm, d_2 = 5 mm, h_2=0.07 mm

5. Conclusions

The paper explored the impact of various structural parameters of the orifice restrictor on the static load-carrying-capacity of hydrostatic gas bearings. The diameter of orifices, thickness of gas film, PEG diameter, and PEG depth were chosen as the experimental factors. The orthogonal test employed the LCC and the MFR as the test indicators. The following conclusions were drawn:

1. The thickness of gas film emerged as the primary test factor influencing the LCC, with the diameter of orifices, PEG diameter, and PEG depth following suit. In terms of the MFR, the diameter of orifices exerted the most substantial impact, followed by the thickness of gas film, while the diameter and depth of PEG exerted lesser influences.

2. The LCC exhibited a direct correlation with the enlargement of both the diameter of orifices and the PEG diameter. Conversely, LCC experienced a reduction when the thickness of gas film was increased. Moreover, LCC underwent an initial increase followed by a subsequent decrease as the PEG depth was augmented. The optimization of LCC was achieved by employing throttle parameters that encompass diameter of orifices of 0.25 mm, thickness of gas film of 0.01 mm, PEG diameter of 5 mm, and PEG depth of 0.07 mm.

3. The MFR showed a gradual increase as the diameter of orifices and thickness of gas film increased. However, the impact of the diameter and depth of PEG on the MFR was not significant. By expanding the diameter and depth of PEG, the MFR experienced a limited range of increase and decrease. The optimized combination of restrictor parameters, in terms of MFR, consisted of diameter of orifices of 0.10 mm, thickness of gas film of 0.01 mm, PEG diameter of 4 mm, and PEG depth of 0.05 mm.

4. Based on the aforementioned findings, the simulation verification experiments were conducted utilizing the ideal parameter configuration of LCC. The results illustrated an increase in LCC by 8% to 709.476 N subsequent to the optimization of the throttle parameters. Furthermore, the MFR experienced a mere 3% growth, reaching 0.0674 g/s. After careful consideration, the most suitable combination of restrictor structure parameters was determined to be as follows: thickness of gas film $h_1 = 0.01$ mm, diameter of orifices $d_1 = 0.25$ mm, PEG diameter $d_2 = 5$ mm, and PEG depth $h_2 = 0.07$ mm.

The paper focused on conducting a simulation study to optimize the structural parameters of the restrictor for hydrostatic gas thrust bearings. Additionally, an experimental setup will be constructed to validate the findings. Future research will aim to enhance the dynamic bearing capacity of gas bearings.

Acknowledgements

The project is supported by the Tongling Major Science and Technology Program (202101JB003), the Anhui Provincial Natural Science Foundation (2308085MF198). Dr. Xinyu Wen and Prof. Yuanlong Chen contributed equally to this work.

Declaration of Interest Statement

The authors declare that they have no conflict of interest.

References

1. **Samsel, M. J.; Chańko, A.; Michałowski, M.; Fernandez-Munoz, M.; Diez-Jimenez, E.** 2023. Tribological Characterization of Micro Ball Bearings with and without Solid-State Lubrication, Micromachines 14: 1775. https://doi.org/10.3390/mi14091775.
2. **Xue, B.; Geng, Y. Q.; Yan, Y. D.; Sun, Y. Z.** 2019. Effects of AFM tip wear on evaluating the surface quality machined by ultra-precision machining process, The International Journal of Advanced Manufacturing Technology 105: 4663-4675. https://doi.org/10.1007/s00170-019-03958-x.
3. **Zhou, Z.; Jia, H.; Yin, B.** 2022. A fully coupled 3D elastohydrodynamic model built with MITC element for static performance analysis of gas foil bearings, Industrial Lubrication and Tribology 74(7): 765-773. https://doi.org/10.1108/ILT-08-2021-0340.
4. **Michalec, M.; Svoboda, P.; Křupka, I.; Hartl, M.** 2021. A review of the design and optimization of large-scale hydrostatic bearing systems, Engineering Science and Technology - an International Journal-JESTECH 24(4): 936-958. https://doi.org/10.1016/j.jestch.2021.01.010.
5. **Luan, W. L.; Liu, Y.; Wang, Y. L.; Xu, F. C.** 2023. Effect of herringbone groove structure parameters on the static performance of gas foil herringbone groove thrust bearings, Tribology International 177: 107979. https://doi.org/10.1016/j.triboint.2022.107979.
6. **Sahto, M. P.; Wang, W.; Sanjrani, A. N.; Hao, C.; Shah, S. A.** 2021. Dynamic Performance of Partially Orifice Porous Aerostatic Thrust Bearing, Micromachines 12: 989. https://doi.org/10.3390/mi12080989.
7. **Gao, Q.; Chen, W. Q.; Lu, L. H.; Huo, D. H.; Cheng, K.** 2019. Aerostatic bearings design and analysis with the application to precision engineering: State-of-the-art and future perspectives, Tribology International 135: 1-17. https://doi.org/10.1016/j.triboint.2019.02.020.
8. **Sahto, M. P.; Wang, W.; Imran, M.; He, L. S.; Li, H.; Gong, W. W.** 2020. Modelling and Simulation of Aerostatic Thrust Bearings. IEEE Access 8: 121299-121310. https://doi.org/10.1109/ACCESS.2020.2999748.
9. **Yu, H. C.; Li, H. H.; Zhao, H. Y.; Ma, W. Q.** 2015. Research on the static characteristics of circular thrust porous aerostatic bearings, 2015 IEEE International Conference on Mechatronics and Automation (ICMA): 1407-1411. https://doi.org/10.1109/ICMA.2015.7237691.
10. **Cui, H. L.; Wang, Y.; Yue, X. B.; Li, Y. F.; Jiang, Z. Y.** 2019. Numerical analysis of the dynamic performance of aerostatic thrust bearings with different restrictors, Proceedings of The Institution of Mechanical Engineers Part J-Journal of Engineering Tribology 233(3): 406-423. https://doi.org/10.1177/1350650118780599.
11. **Khan, P. V.; Segu, D. Z.; Hwang, P.** 2017. The effect of the arc on annular-thrust aerostatic porous bearings, Industrial Lubrication and Tribology 69(6): 925-929. https://doi.org/10.1108/ILT-12-2016-0310.
12. **Nishio, U.; Somaya, K.; Yoshimoto, S.** 2011. Numerical calculation and experimental verification of static

and dynamic characteristics of aerostatic thrust bearings with small feedholes, Tribology International 44(12): 1790-1795. https://doi.org/10.1016/j.triboint.2011.07.004.
13. **Chen, X. D.; He, X. M.** 2006. The effect of the recess shape on performance analysis of the gas-lubricated bearing in optical lithography, Tribology International 39(11): 1336-1341. https://doi.org/10.1016/j.triboint.2005.10.005.
14. **Faraj, Z.; Aboussaleh, M.; Zaki, S.; Abouchadi, H.; Kabiri, R.** 2022. Optimization of the parameters of the selective laser sintering for the formation of PA12 samples by the Taguchi method, International Journal of Advanced Manufacturing Technology 122: 1669-1677. https://doi.org/10.1007/s00170-022-09991-7.
15. **Adar, E.; Acar, F. N.** 2021. Adsorption of textile wastewater containing triple dye on the garden soil: optimisation and modelling by Taguchi method, International Journal of Environmental Analytical Chemistry 103(19): 7945-7960. https://doi.org/10.1080/03067319.2021.1977929.
16. **Akbari, M.; Asadi, P.** 2021. Optimization of microstructural and mechanical properties of brass wire produced by friction stir extrusion using Taguchi method, Proceedings of the Institution of Mechanical Engineers, Part L: Journal of Materials: Design and Applications 235(12): 2709-2719. https://doi.org/10.1177/14644207211032992.

Y. Chen, X. Wen, Y. Wang, M. Wu, J. Zhou, S. Wanyan

OPTIMIZATION OF RESTRICTOR PARAMETERS AND STATIC CHARACTERISTICS STUDY ON ORIFICE TYPE HYDROSTATIC THRUST BEARING

S u m m a r y

Gas bearings play a crucial role in maintaining the precision of ultra-precision machine tools. However, the bearing capacity is inferior to that of rolling bearings. The bearing capacity of gas bearings is directly influenced by restrictor structural parameters. To clarify the combined effect of restrictor structural parameters on the static bearing capacity of gas bearings and enhance the bearing capacity. The orthogonal test method was used to investigate the impact of various combinations of parameter levels (e.g. diameter of orifices d_1, thickness of gas film h_1, diameter d_2 of pressure-equalizing groove (PEG), and PEG depth h_2 on the static load-carrying-capacity of the bearings). The load-carrying-capacity (LCC) and mass flow rate (MFR) were selected as the experimental indicators. Results showed that gas film thickness, orifice diameter, PEG diameter and PEG depth dominated LCC. Additionally, it was observed that diameter of orifices has the most significant impact on MFR, followed by thickness of gas film, PEG diameter, and PEG depth having the smallest influence on MFR. LCC serves as a critical manifestation of the static bearing capacity of bearings. However, this increase in LCC unavoidably resulted in higher gas consumption, leading to an elevated MFR. Consequently, the structural parameters of restrictor were optimized based on the principle of optimal LCC, while also ensuring that there was no significant rise in MFR. The optimized parameter combinations were thickness of gas film $h_1 = 0.01$ mm, diameter of orifices $d_1 = 0.25$ mm, PEG diameter $d_2 = 5$ mm, and PEG depth $h_2 = 0.07$ mm. This study can contribute to a profound understanding of the nonlinear dynamic mechanism and structural optimization design application of air bearing.

Keywords: restrictor, hydrostatic gas bearings, orthogonal test, analysis of variance, LCC.

Received May 14, 2024
Accepted December 16, 2024